AIAA JOURNAL
Vol. 39, No. 12, December 2001

Spacelab Experiments on Combustion of Heptane/Hexadecane Droplets

Benjamin D. Shaw,* Bret D. Clark,† and Difei Wang‡
University of California, Davis, Davis, California 95616

Results are presented from experiments on reduced-gravity combustion of individual heptane/hexadecane droplets. Initial droplet diameters ranged from 0.25 to 5.2 mm, and initial hexadecane mass fractions in the droplets were 0.058, 0.10, 0.20, and 0.40. Most droplets were burned in cabin air on Spacelab with an ambient oxygen mole fraction of about 0.21 and a pressure of about 0.1 MPa. Data were also obtained for small (0.25-mm) droplets in a ground-based apparatus that provides simulated reduced gravity environments for droplet combustion experiments. Droplets in this apparatus were burned in high-temperature gases at 0.1 MPa. Data on flame contraction (i.e., the sudden contraction of the flame from droplet heating as the surface liquid mass fraction rapidly approaches unity) were used to estimate effective liquid species diffusivities that apply to these droplets. Significant differences in effective liquid species diffusivities were observed; these differences may be related to variations in internal circulation within the droplets, as well as possible variations in droplet temperatures. The Spacelab results indicate that flame extinction can be induced by flame contraction and that the occurrence of extinction depends on the initial droplet size. It was also observed that sooting and radiant heat losses varied significantly with initial droplet size in the Spacelab experiments. Sooting decreased as initial droplet sizes increased, whereas radiant heat loss rates varied in a complex fashion with the initial droplet size.

Nomenclature

D	=	effective liquid species diffusivity
d	=	instantaneous droplet diameter
d_c	=	droplet diameter at the onset of flame contraction
d_0	=	initial droplet diameter
g_0	=	normal gravitational acceleration, 9.81 m/s^2
H_0	=	variable defined after Eq. (5)
H_1	=	variable defined after Eq. (5)
H_2	=	variable defined after Eq. (5)
h	=	heat of combustion
h_{match}	=	variable defined after Eq. (5)
h_0	=	variable defined after Eq. (5)
h_1	=	variable defined after Eq. (5)
K	=	instantaneous burning-rate constant (based on droplet diameter)
K_1	=	burning-rate constant (based on droplet diameter) before the onset of flame contraction
L	=	enthalpy of vaporization of the high-volatility component
m	=	fuel mass flow rate off of the surface of a droplet
Q_{chem}	=	instantaneous chemical heat release that is made available by fuel vaporization
Q_{rad}	=	radiant heat loss rate (based on either rad 1 or rad 2 data)
q	=	radiometer heat flux reading (from rad 1 or rad 2)
R	=	gas constant for the high-volatility component
r	=	distance from the center of the radiometer to the center of the bead at the deployment site
T_b	=	boiling point of the initial liquid mixture comprising a droplet
T_c	=	droplet temperature at the onset of flame contraction [see Eq. (6)]
T_0	=	initial droplet temperature
t	=	time
Y	=	initial mass fraction of the low-volatility component in a droplet
β'	=	small parameter representing the ratio of a characteristic time for droplet temperature changes to a characteristic time for droplet size changes (before flame contraction)
ε	=	$8D/K_1$
θ	=	angle that either radiometer is tilted relative to the bead where a droplet was deployed
ρ	=	liquid density
τ	=	dimensionless time, $\ell n(d_0/d)$
τ_c	=	dimensionless time at the onset of flame contraction, $\ell n(d_0/d_c)$
ω	=	ratio of the molecular weights of the high-volatility and low-volatility components

Received 14 April 2000; revision received 15 June 2001; accepted for publication 21 June 2001.

*Professor, Mechanical and Aeronautical Engineering Department.
†Research Assistant, Mechanical and Aeronautical Engineering Department; currently Instructor, Lucia Mar USD, Grover Beach, CA 93420.
‡Research Assistant, Mechanical and Aeronautical Engineering Department; currently Combustion Engineer, Cheng Power Systems, Mountain View, CA 94040.

Introduction

LIQUID fuels are usually burned in the form of sprays, with initial droplet sizes in the range 50–100 μm or smaller. In dense sprays, droplet–droplet interactions are important, and flames can exist around groups of droplets. Droplets can also burn individually in sufficiently dilute sprays. Because of the enormous practical importance of spray combustion, much effort has been directed toward increasing understanding of bulk spray processes as well as behaviors of individual droplets. Although much is known about gasification and combustion of droplets, there are aspects of the fundamental processes for which additional basic knowledge is needed if thorough interpretations and explanations are to be obtained. For example, effects of liquid-phase species diffusion rates on unsteady burning, effects of gas-phase unsteadiness, effects of sooting and radiation, and conditions for extinction are of interest. In addition, increasing basic knowledge of droplet combustion phenomena can provide information that is useful for developing and validating models of combustion of liquid fuels in practical combustion systems. For example, the results described herein provide information on effective liquid species diffusivities in burning droplets; liquid species diffusivities have been recognized as being important in determining gasification behaviors of multicomponent droplets.[1–7]

The present research is concerned with studying combustion of individual droplets composed of mixtures of heptane and hexadecane.

These species were selected because they differ significantly in volatility and they were expected to display sudden flame contractions that can occur in droplets composed of species with widely differing volatilities. Sudden flame contractions occur as a result of the rapid buildup of the low-volatility component at the droplet surface. This buildup leads to droplet heating, causing temporary decreases in droplet vaporization rates and flame diameters as a droplet heats.[8–10] (The flame may also become cooler during the reduced vaporization period, which will contribute to flame size reductions.)

Flame contractions were of interest in this study. Theoretical expressions that assume spherical symmetry have been developed[9] and extended[10] to analyze conditions leading to the onset of flame contraction. The extended theory[10] is used here to estimate effective liquid species diffusivities for heptane/hexadecane droplets, initially up to 5.2 mm in diameter, burned in Spacelab droplet combustion experiments during the 1995 flight of the Second United States Microgravity Laboratory (USML-2) and the 1997 flight of the First Microgravity Science Laboratory (MSL-1). The theory is also used to estimate effective liquid species diffusivities in ground-based experiments with initially smaller heptane/hexadecane droplets. In the experiments, the droplets likely experienced internal convective flows that were strong enough to influence liquid species transport. This is why the terminology effective diffusivity is used here, that is, because species transport inside droplets was likely influenced by convection. As described later, these convective flows may have resulted from effects related to formation and (asymmetric) ignition of droplets, as well as capillary flows caused by the presence of a support fiber that was used in the Spacelab experiments. In addition, note that the data presented herein indicate that extinction of large droplets can be induced by flame contractions and that the occurrence of extinction depends on the initial droplet diameter.

It was found in the Spacelab experiments that sooting and radiant heat losses varied strongly with initial droplet sizes. Although of fundamental interest, these observations are also potentially relevant to spacecraft fire safety issues in that sooting decreased as the droplet flames became larger, which is contrary to many normal gravity results. In addition, the spectral (radiant emission) characteristics of the flames changed as their sizes increased. These characteristics may be present in other microgravity flames, and as such, space-based fire detection techniques may need to take these behaviors into account. It is also the opinion of the authors that studies of large and easily observable droplets, such as those considered here, can provide fundamental information on droplet behaviors. When theory and experiment agree for experiments such as these, then predictions for cases where accurate experimental data are lacking (as in many liquid fuel combustion systems) can be made with more confidence.

Note that previous experimental results have been reported for combustion of heptane/hexadecane droplets in reduced gravity, though for conditions different from those reported here. Yang and Avedisian[11] studied combustion of heptane/hexadecane droplets in a drop tower. The droplets, which were burned in air at 0.1 MPa, were initially about 0.5 mm or smaller. Aharon and Shaw[10] studied combustion of heptane/hexadecane droplets initially about 1 mm in diameter in a drop tower; the droplets were burned in various environments with pressures that ranged from 0.03 to 0.3 MPa. Mikami et al.[12] have reported results from combustion of heptane/hexadecane droplets, initially about 1 mm in diameter, at pressures up to 3 MPa. Finally, Dietrich et al.[13,14] have presented preliminary results from Spacelab experiments on combustion of heptane/hexadecane droplets initially up to about 5.2 mm in diameter; these droplets were burned in Spacelab cabin air at about 0.1-MPa pressure. The present experiments extend the previous studies, specifically addressing different fuel mixture ratios and droplet sizes and providing further analyses of the USML-2 experiments. In addition, the MSL-1 experiments employed radiometers for measurement of radiant heat loss rates during microgravity droplet combustion. These types of measurements have been reported only for initially smaller single-component droplets burned in a drop tower.[15] Also note that computational results have been presented on combustion of heptane/hexadecane droplets in microgravity, with nonluminous radiant heat loss effects included.[16]

Experimental Methodology

The Spacelab experiments utilized the Glovebox Facility located in the Spacelab module of the space shuttle. The Glovebox Facility is a general-purpose facility that provides power and video capabilities to small-scale experiments. The crews conducted several small-scale experiments inside this facility during the STS-73 (USML-2) and STS-94 (MSL-1) missions. The USML-2 experiments made use of the fiber supported droplet combustion (FSDC) apparatus, and the MSL-1 experiments used the FSDC-2 apparatus. For clarity, FSDC will be referred to as FSDC-1 in the following text. In both the FSDC-1 and FSDC-2 experiments, various droplet compositions, including heptane/hexadecane mixtures, were studied by several different investigators.[13,14,17] The present paper gives results on the heptane/hexadecane droplet combustion experiments. Six heptane/hexadecane droplets were burned in the FSDC-1 experiments. Five of these droplets had an initial hexadecane mass fraction Y of 0.4 and the other droplet had $Y = 0.1$. There were 22 heptane/hexadecane droplets burned in the FSDC-2 experiments. Of these droplets, 11 had $Y = 0.058$ and the remainder $Y = 0.20$. Most of the FSDC-2 experiments yielded data that were useful for the purposes of this paper, and these data are described herein along with data from the FSDC-1 experiments.

Details on the FSDC-1 apparatus are presented elsewhere[13,14] (as are some preliminary FSDC-1 results), and only a short description of this apparatus is provided here. In the FSDC-1 heptane/hexadecane experiments, individual droplets were deployed onto a silicon-carbide support fiber (80-μm diam). The droplets were ignited using a single wire loop ignitor, and orthogonal flame and droplet views were provided by two video cameras. The droplet view was backlit, and the flame view was not. Whereas most FSDC-1 experiments were performed in a quiescent environment, one droplet was burned in a convective flow with a uniform air speed of 30 mm/s. Data were recorded onto videotape and analyzed after the flight using digital image analysis techniques described elsewhere.[13] The errors in droplet size measurements are estimated to be about 5% or less. For both FSDC-1 and FSDC-2, droplets were burned in cabin air at pressures of about 0.1 MPa and with oxygen mole fractions of about 0.21. Residual gravity levels during the burns were typically about $1 \times 10^{-5}\ g_0$ or lower, and rms gravity levels were typically about $2 \times 10^{-4}\ g_0$ or lower, where $g_0 = 9.81$ m/s^2.

The FSDC-2 apparatus was similar to the FSDC-1 apparatus, though one difference is that two radiometers were added to allow measurements of radiant heat fluxes.[17] One radiometer (denoted as this paper as rad 1) measured incident radiant power over the wavelength range from 0.6 to 40 μm. Rad 1 was a Dexter thermopile detector (Model 2M). The time constant for this radiometer was 85 ms, and the view angle was 80 deg. The other radiometer (rad 2), which was also obtained from Dexter (Model 2M), employed a Spectragen filter (model number LP-5100-F) to measure incident radiant power over the wavelength range from 5.1 to 7.5 μm. This range corresponds approximately to radiant emission from a water vapor emission band. The time constant for rad 2 was 85 ms, and the view angle was 80 deg. The radiometer view angles were sufficient to allow the droplet flames to be within the radiometer fields of view during the combustion periods. The radiometers, which were located near the bottom of the FSDC-2 module, were pointed directly at the bead location at the midpoint of the deployment fiber, which is where the $Y = 0.058$ droplets were burned. The $Y = 0.20$ droplets were burned at a bead location 5 mm away from the midpoint bead. The distance from each radiometer to the bead at the fiber midpoint was about 74.5 mm, and the radiometers were essentially symmetrically located on either side of the fiber midpoint. The angle between the radiometer centerline views was 14 deg, that is, if a line were drawn extending out from each radiometer, the lines would intersect with an angle of 14 deg. A schematic of the geometry of the radiometers relative to the fibers is shown in Fig. 1. Calibration of the radiometers was performed by NASA with a blackbody radiation source. The radiometers allowed measurement of the radiant heat flux that was incident on each detector.

Another difference is that small beads (roughly 400-μm diam normal to the fiber) were placed on the fibers in the FSDC-2 apparatus to minimize droplet drift along the fiber. The fibers in the

Table 1 Results obtained from FSDC-1 and FSDC-2 heptane/hexadecane droplet combustion experiments

Test	Y	d_0, mm	K_1, mm^2/s	ε	$D \times 10^9$, m^2/s
1	0.10	4.60	0.39	0.23	11
2	0.058	1.80	0.60	0.098	7.4
3	0.058	2.05	0.61	0.081	6.2
4	0.058	2.21	0.60	0.066	5.0
5	0.058	2.77	0.55	0.18	12
6	0.058	2.86	0.52	0.097	6.3
7	0.058	3.86	0.34	0.24	10
8	0.058	4.74	0.40	0.27	14
9	0.058	4.85	0.41	0.26	13
10	0.058	5.24	0.41	0.22	11
11	0.20	2.53	0.60	0.093	7.0
12	0.20	2.93	0.30	0.26	9.8
13	0.20	3.63	0.19	0.28	6.7
14	0.20	3.81	0.22	0.37	10
15	0.20	4.49	0.24	0.34	10
16	0.20	4.53	0.23	0.28	8.1
17	0.20	4.60	0.25	0.33	10
18	0.40	3.0	0.67	0.13	11
19	0.40	3.4	0.39	0.25	12
20	0.40	3.5	0.43	0.35	19
21	0.40	3.9	0.44	0.18	10
22	0.40	5.2	0.38	0.36	17

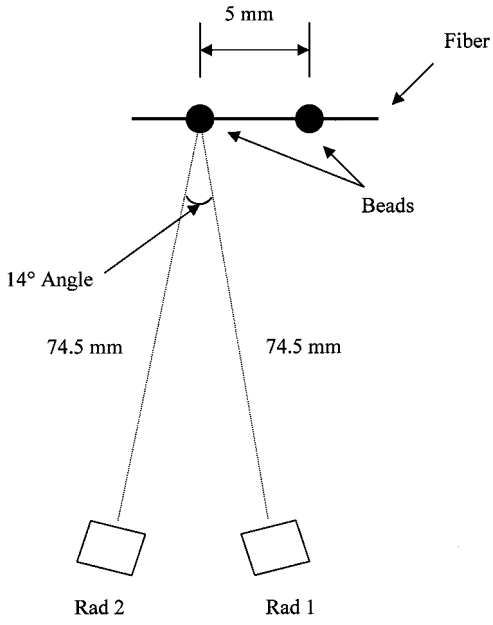

Fig. 1 Schematic of positions of radiometers relative to deployment fiber beads (not drawn to scale); for clarity, only beads used in experiments described in this paper are shown.

FSDC-1 experiments were not beaded. Both 80- and 150-μm fibers were used in the FSDC-2 experiments. The $Y = 0.058$ droplets were burned on 80-μm fibers, and the $Y = 0.20$ droplets were burned on 150-μm fibers. Different fiber sizes were used because of operational issues encountered during the space flight. During the experiments the droplets sometimes moved back and forth along the fiber, though droplet movements were restricted because of the beads in the sense that the liquid/gas interface at the surface of a droplet could not move past a bead (because of surface tension effects). Image analysis methods for the FSDC-2 experiments were the same as for the FSDC-1 experiments. Test conditions and results for both FSDC-1 and FSDC-2 are summarized in Table 1. Each test in Table 1 corresponds to a specific experiment.

The ground-based experiments utilized a drop-tube apparatus that provides reduced-gravity conditions for smaller droplets (initial diameters of about 0.25 mm) in a ground-based laboratory setting. This apparatus is described in detail elsewhere,[18] and only a brief description is given here. With this apparatus, the hot gases from a flat-flame burner were directed down a vertical tube of variable cross section. The tube walls were contoured to accelerate the centerline flow at the gravitational acceleration, providing an environment where buoyancy effects were greatly reduced because centerline pressure gradients were reduced to very low levels. Widely spaced droplets were injected into the flow tube such that their velocity profiles closely matched the centerline velocity profile in the tube. As a result, the droplets in the tube experienced greatly reduced buoyant and forced convective flows, that is, spherical symmetry was strongly promoted.

As has been shown elsewhere,[18] use of this apparatus has yielded fundamental results on behaviors of single component droplets. This apparatus has been used in the present research to provide data on combustion of small heptane/hexadecane droplets (initially about 0.25 mm) under reduced-gravity conditions. Droplets were burned in environments at 0.1 MPa and about 1073 K. The environment composition was 21% O_2, 35.9% N_2, 14.4% CO_2, and 28.7% H_2O (on a molar basis). Effective gravity levels were about 10^{-3} g_0, and droplet–gas Reynolds numbers (based on the droplet diameter) were about 0.02 or less. As a result, buoyant and forced convection effects were negligible. If the contoured tube was not used, effective gravity levels would be about 10^3 times larger, and droplet–gas Reynolds numbers would be of order unity. Droplets were spaced about 150 initial droplet diameters apart such that droplet–droplet interactions were negligible. Video images of droplets were analyzed using techniques described elsewhere.[18] Errors in droplet size measurements are estimated to be about 5% or less.

Experimental Results

Figures 2 and 3 show representative radiometer data and droplet size data for the droplets burned in the FSDC-2 experiments. Representative plots of droplet diameter histories from the FSDC-1 experiments are presented elsewhere.[13,14] Because of the large number

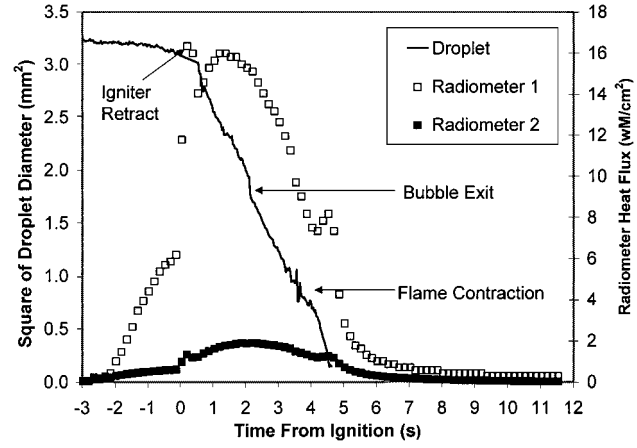

Fig. 2 Droplet diameter data and radiometer data for an FSDC-2 heptane/hexadecane mixture droplet ($Y = 0.058$, $d_0 = 1.80$ mm, and test 2 in Table 1).

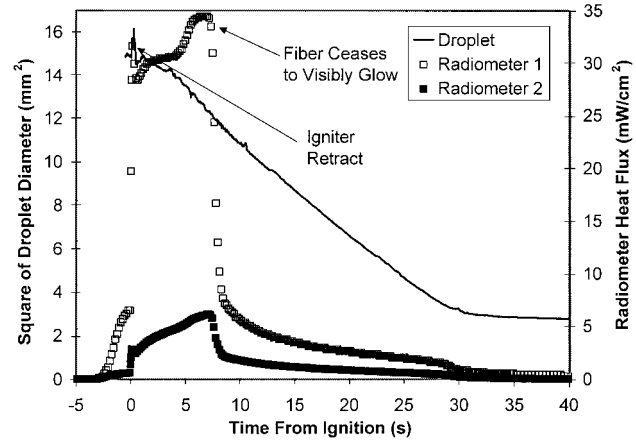

Fig. 3 Droplet diameter data and radiometer data for an FSDC-2 heptane/hexadecane mixture droplet ($Y = 0.058$, $d_0 = 3.86$ mm, and test 7 in Table 1).

of droplets burned in the FSDC-2 experiments, only representative plots of FSDC-2 droplet size histories and radiometer histories are presented here.

Radiometer data and data for the square of the droplet diameter d are shown as a function of the time t from ignition in Fig. 2 for a droplet ($Y = 0.058$) initially about 1.8 mm in diameter. After ignition, the d^2–t plot is basically (although not precisely) linear until an interior bubble exits the droplet, causing a sudden but small decrease in droplet size (the bubble exit was clearly evident in the video record, allowing the time of the bubble exit to be easily measured). For reasons that are not clear, small bubbles were present in many of the Spacelab heptane/hexadecane droplets before ignition; these bubbles often exited the droplets while the droplets were burning. After the bubble exits, the d^2–t plot is again basically linear with about the same average slope as before the bubble exit. The d^2–t data also exhibit a temporary and mild decrease in slope at about 3.5 s; this decrease is related to the flame contraction, which was evident from flame size variations and changes in the location of the fiber glow, as described later. The scatter in the d^2–t data evident in Fig. 2 (and also in Figs. 3–5) is a result of droplet movements along the fiber (about the bead) as well as sometimes from the exit of small bubbles from the droplets.

Although many of the droplets had small bubbles, it is likely that the effects of these bubbles were small (because of their small sizes). Note, however, that bubbles would affect transport of energy and mass in the liquid phase by introducing small local inhomogeneities. Also, as noted earlier, the exit of a bubble from a droplet can cause sudden (and typically small) decreases in droplet sizes. The bubbles were also useful in the sense that they provided indications of flows inside droplets. These flows generally appeared to be random. Interestingly, the flows, as visualized by the bubbles, generally decayed very quickly after flame extinction, which may indicate the presence of Marangoni effects. Also note that, because of their small sizes and also because they were not easily imaged, the bubbles generally could not be seen clearly enough to determine details about their behaviors, for example, growth from droplet heating.

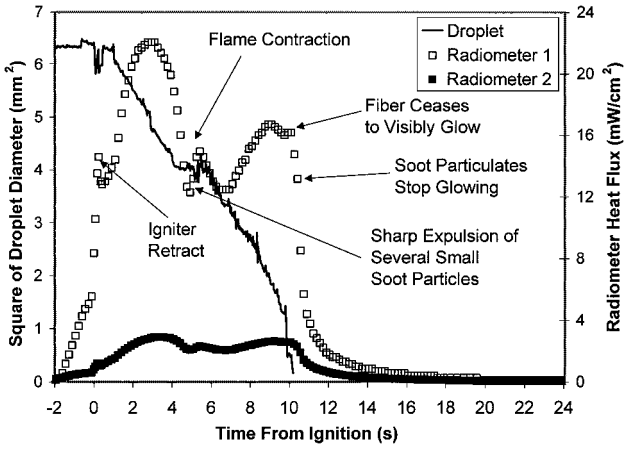

Fig. 4 Droplet diameter data and radiometer data for an FSDC-2 heptane/hexadecane mixture droplet ($Y = 0.2$, $d_0 = 2.53$ mm, and test 11 in Table 1).

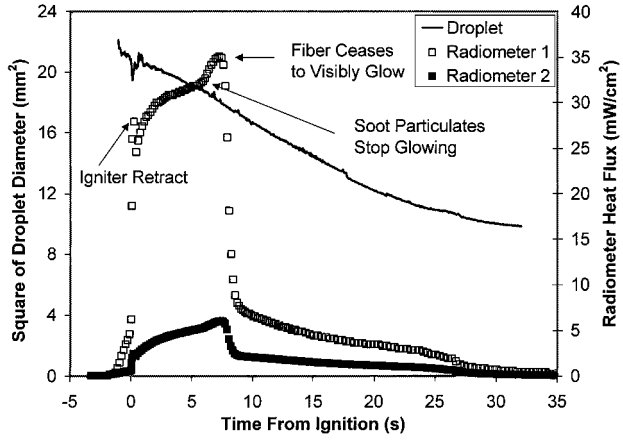

Fig. 5 Droplet diameter data and radiometer data for an FSDC-2 heptane/hexadecane mixture droplet ($Y = 0.2$, $d_0 = 4.53$ mm, and test 16 in Table 1).

As noted earlier, d^2–t data for the droplet in Fig. 2 appear to display staged combustion where two periods of approximately d-square law combustion (i.e., where the square of the droplet diameter decreases linearly with time) are separated by a time period where vaporization rates are decreased; the decrease in vaporization rates is sometimes termed a plateau. The onset of the plateau has been observed in ground-based experiments to closely coincide with flame contractions associated with rapid droplet heating when the liquid surface mass fraction of hexadecane closely approaches unity. This is expected to apply here, as well. For some droplets, a plateau was clearly evident in the d^2–t plots (for example, Fig. 4), and in others a plateau was difficult to discern from the d^2–t plots (Fig. 2). As discussed elsewhere,[10] it can sometimes be difficult to determine flame contraction onset times based on d^2–t data alone, and it is usually desirable to measure onset times for flame contraction from images of flames in conjunction with d^2–t data. In the present experiments this was not always possible because the larger droplets had very weak flames that could not be imaged by the video cameras, though the flames of the smaller droplets could be imaged, as discussed hereafter. When flames could not be imaged, times for flame contraction were estimated from the d^2–t data when possible. The radiometer data were also sometimes useful in this regard. In addition, it was assumed that extinction, when present, was induced by flame contraction.

Similar to the FSDC-1 experiments,[13,14] which dealt with large droplets initially from 3.0 to 5.2 mm in diameter, it was found that the flames of the larger FSDC-2 heptane/hexadecane droplets were very dim and could be imaged by the video cameras only for short time periods after ignition. Unlike alcohol droplets burned in the other FSDC-1 and FSDC-2 experiments,[13,14,17] glowing of support fibers was not evident (except for time periods of a few seconds following ignition) in the video images of larger heptane/hexadecane droplets, suggesting that the flame temperatures were very low for the larger droplets. The smaller FSDC-2 droplets behaved differently, however. For example, for the droplet in Fig. 2, the fiber glow was visible throughout the burning history, allowing direct observation of the flame contraction as evidenced by a sudden and temporary decrease in the distance between the droplet center and the regions of the fiber that were glowing. The flame contraction period, as observed in the flame image video, is noted in Fig. 2. Soot radiation in the form of a thick luminous yellow zone between the droplet and the flame, and which lasted over most of the lifetime of this droplet, was also evident on the video records. This yellow zone dimmed temporarily and showed a sudden and temporary decrease in diameter when the flame contraction occurred. These behaviors are consistent with drop tower experiments[10] that employed heptane/hexadecane droplets initially about 1 mm in diameter.

Note that flame contraction is expected to occur when most of the heptane is depleted from the droplet surface.[8–10] If the droplet were well mixed during its combustion history, the ratio $(d_c/d_0)^2 = Y^{2/3}$ would be expected to apply under well mixed conditions, where d_c is the droplet diameter at the onset of flame contraction and d_0 the initial droplet diameter. In the present experiments, however, the droplets were likely not well mixed because characteristic droplet lifetimes are short relative to characteristic lifetimes for liquid species diffusion. As a result, flame contraction should occur before all of the heptane has been depleted from a droplet (though flame contraction will occur when the heptane has been depleted from the droplet surface). Because of the limited liquid species transport rates, there will still be heptane in the droplet interior at the time of flame contraction, leading to values of $(d_c/d_0)^2$ that are larger than $Y^{2/3}$. For example, for the data in Fig. 2, the value $(d_c/d_0)^2 \approx 0.3$ applies (after accounting for the bubble exit) while $Y^{2/3} = 0.058^{2/3} = 0.15$, indicating that heptane was still present in this droplet at the onset of flame contraction. This type of behavior

is exploited later in this paper to provide estimates of effective liquid species diffusivities for these droplets using an analytical approach.

The radiometer data in Fig. 2 show increases after the ignitor was turned on (about 2 s before ignition), sharp increases after droplet ignition, and decreases after the ignitor is turned off and retracted. Following ignition, radiant heat fluxes grow and then decrease, with an increasing rate of decrease at the time of the flame contraction. After the flame contraction, the radiometer readings increase again for a short while before droplet burnout occurs. Interestingly, the shapes of the curves for these radiometer data (especially rad 1) are qualitatively similar to flame diameter data published for drop-tower experiments with heptane/hexadecane droplets initially about 1 mm in diameter.[10] During a flame contraction, the soot would have been driven inward, from thermophoretic forces, to cooler regions near the droplet.[19] At the same time, the hot gases around the flame zone may have cooled during the flame contraction because the heat release rate in the flame zone would have been reduced, and any soot remaining near the flame zone would have cooled as well. These factors would have reduced radiant heat emissions, as sensed by the radiometers. After the flame contraction, the gases and soot near the flame zone would have heated and soot would have accumulated in hotter regions near the flame, leading to the increases in radiant emissions observed in the experiments.

Figure 3 reports d^2–t and radiometer data for a larger droplet ($Y = 0.058$) initially about 3.86 mm in diameter. Similar to the largest droplet burned in the FSDC-1 experiments,[13] the d^2–t plot for this droplet is fairly linear until a certain time in the burning history, at which time the d^2–t data level off (about 29 s in Fig. 3). The radiometer data for this droplet are different than for the initially smaller droplet shown in Fig. 2. As would be expected, the radiometer values are larger for the larger droplet (Fig. 3), at least at early times. At about 7 s into the burning history, however, the radiometer measurements in Fig. 3 show sudden and steep declines in their values. At this time, the radiometer readings drop to values that are less than for the smaller droplet in Fig. 2. Before about 7 s, the larger droplet displayed radiant soot emissions that could be clearly discerned in the videos. After ignition, a spherical yellow luminous zone was evident between the droplet and the flame. This luminous zone dimmed over a period of about 2 s such that it could not be imaged by the video camera. Following this, however, glowing of large soot particulates could be seen in the video images for several seconds longer. When all radiant soot emissions disappeared and glowing of the fiber was no longer visible, the radiant emissions from the flame were likely not dominated by broadband emissions from soot, but rather by band emissions from gaseous combustion products, which would have been much weaker.

This conclusion is supported by noting that before about 7 s in Fig. 3, the heat flux readings from rad 1 were 6 to 7 times higher than for rad 2. After about 7 s, however, the readings for rad 1 are only about 2 to 3 times higher than for rad 2, which is reasonable because the major gas-phase radiant species should be CO_2 and H_2O, and these species will have effective emissivities that are about the same. This is based on the assumption that the partial pressures of these two species will be similar in the high-temperature region around the primary reaction zone. Before about 7 s, when significant soot radiation was present, it is to be expected that the broadband radiation from soot emissions will result in higher heat flux readings for rad 1 than for rad 2. This is also evident in Fig. 2, where the rad 1 heat fluxes are about 7 to 8 times higher than the rad 2 heat fluxes; the data in Fig. 2 are for a droplet that had significant soot throughout its history.

Based on simple scaling estimates, it is clear that in the first approximation heat release rates will scale approximately with the droplet diameter whereas radiant heat loss rates will scale approximately with the cube of the droplet diameter (assuming a constant flame temperature and a quasi-steady gas phase). As a result, droplet flames should become cooler as droplet sizes increase. This can lead to reduced burning rates, reduced sooting, and extinction from radiant heat losses.[13,15,16,20–23] The flame of the larger droplet mentioned earlier was apparently hot enough shortly after ignition to produce significant amounts of soot and to cause observable fiber glows. As this flame grew in size, however, radiant heat losses would have become more significant, and, when the flame was large enough, radiant heat loss rates would have caused the flame to be too cool to produce significant amounts of soot. Sufficiently small droplets do not have flames so large that they become too cool to produce soot. These factors explain the trends in the radiometer data in Figs. 2 and 3.

Also note that the leveling off of the Fig. 3 d^2–t plot at about 29 s corresponds to when the radiometer readings begin to rapidly approach zero, indicating that extinction occurred. Flame extinction generally occurred with the larger droplets burned in the FSDC-1 and FSDC-2 experiments. Following extinction of a droplet, a haze appeared that obscured the view of the droplet. This haze is likely an aerosol that nucleated from either unburned fuel vapor or possibly water vapor produced during the combustion.[16] The radiometer data in the FSDC-2 experiments verified that the haze appeared after extinction, indicating that the haze was not soot, as had been originally postulated.[13]

Figures 4 and 5 show analogous data for the $Y = 0.20$ FSDC-2 droplets. In these plots, the same qualitative trends are apparent in the d^2–t data and radiometer readings as for the $Y = 0.058$ droplets. One important difference, however, is that the flame contractions occurred at earlier times in the sense that the ratio of the droplet diameter at the onset of flame contraction d_c to the initial droplet diameter d_0 was larger for $Y = 0.20$ than for $Y = 0.058$. This behavior is expected,[9,10] and, in fact, measurements of d_c/d_0 and K_1 can be used to provide estimates of the effective liquid species diffusivities that apply to these experiments, as described in the next section.

The rate that heat is lost via radiation, Q_{rad}, is estimated using

$$Q_{\text{rad}} = \frac{4\pi r^2 q}{\cos(\theta)} \tag{1}$$

where r is the distance from the radiometer center to the droplet center (which is taken as the location of the bead at the deployment site), q the radiometer heat flux reading, and θ the angle the radiometer is tilted relative to the bead center. In writing Eq. (1), it is assumed that the thermal radiation field is spherically symmetrical (estimates indicate that radiant heat fluxes from the support fibers were small and may be neglected). In the following, both rad 1 and rad 2 will be used to provide values for Q_{rad} in Eq. (1). When rad 1 data are used, Q_{rad} provides values for the total radiant heat loss rate from a flame. When rad 2 data are used, Q_{rad} provides values for the radiant heat losses from a flame in the wavelength range from 5.1 to 7.2 μm.

It is of interest to compare radiant heat loss rates with gas-phase chemical heat release rates. Ideally, chemical heat release rates should be determined for the entire gas phase. In the present case, however, we do not have experimental data that allow for this. It is also reasonable to assume that chemical heat release rates will scale in some way with the flame size, though transient effects, for example, fuel vapor accumulation, would need to be accounted for. Because the flames in the present experiments were not always visible, this approach is also not workable. As a result, we will define the variable Q_{chem} to be the instantaneous chemical heat release that is made available by vaporization of fuel from the droplet surface [see Eq. (2) hereafter], and Q_{rad} will be compared with Q_{chem}:

$$Q_{\text{chem}} = mh \tag{2}$$

In Eq. (2), m is the fuel mass flow rate off of the droplet surface and h is the heat of combustion. Equation (2) gives the chemical heat release that would occur with a quasisteady gas phase (and if complete combustion occurred). Even though the flames were not quasi steady in the present experiments, it is expected that Eq. (2) will provide reasonable estimates for chemical heat release rates.

The fuel mass flow rate is calculated using the following equation:

$$m = (\pi/4) K d \rho \tag{3}$$

In Eq. (3), K is the instantaneous burning rate constant (based on droplet diameter), d the instantaneous droplet diameter, and ρ the liquid density. Combining Eqs. (1–3) yields the following expression for the fraction of the chemical heat release that is lost to radiant emission:

$$\frac{Q_{\text{rad}}}{Q_{\text{chem}}} = \frac{16 r^2 q}{\rho h K d \cos(\theta)} \tag{4}$$

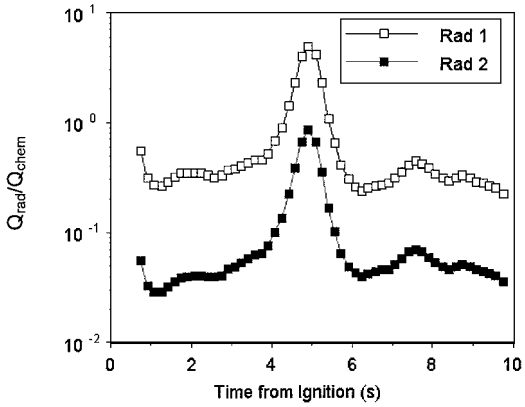

Fig. 6 Data on the ratio Q_{rad}/Q_{chem} obtained from FSDC-2 experiments ($Y = 0.2$, $d_0 = 2.53$ mm, and test 11 in Table 1).

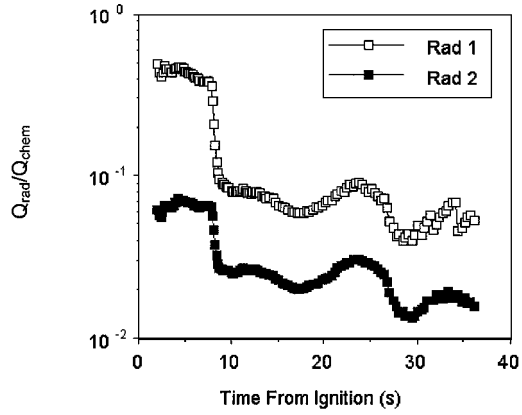

Fig. 7 Data on the ratio Q_{rad}/Q_{chem} obtained from FSDC-2 experiments ($Y = 0.2$, $d_0 = 4.53$ mm, and test 16 in Table 1).

For the FSDC-2 experiments, Eq. (4) yields the result that the ratio Q_{rad}/Q_{chem} varied significantly with the initial droplet size. Representative data are shown in Figs. 6 and 7 for small and large droplets, respectively. The radiometer data in Fig. 6 are from test 11, whereas the data in Fig. 7 are from test 16. In calculating these data, the values $\rho = 700$ kg/m^3 and $h = 45 \times 10^3$ kJ/kg were used. In addition, instantaneous K values were determined from the data by calculating the slopes of best-fit lines though 10–20 data points centered about each time where K was calculated. This procedure allowed reasonable values of K to be determined, while at the same time filtering out most errors that are introduced by differentiating experimental data that invariably have some noise. Whereas errors in the radiometer measurements are estimated to be in the 5% range, errors in calculating the ratio Q_{rad}/Q_{chem} are estimated to be about $\pm 20\%$ or possibly higher because of uncertainties in determining instantaneous burning rates. In both Figs. 6 and 7, data are plotted only during the periods while droplets were burning.

Figure 6 shows that Q_{rad}/Q_{chem} is roughly in the range from 0.3 to 0.4 for most of the burning history, except during the flame contraction period where Q_{rad}/Q_{chem} achieves a peak value of about 6. The presence of a peak is expected based on the definition of Q_{chem} because burning rates are low during the flame contraction period. Note that similar Q_{rad}/Q_{chem} values for microgravity combustion of heptane droplets in air at 1 atm have been reported.[15] These heptane droplets were initially about 1.3 m in diameter.

In contrast, the data in Fig. 7 show different behaviors. After ignition, the Q_{rad}/Q_{chem} values are in the range 0.4 to 0.6, which is to be expected because these droplets are larger. At about 8 s after ignition, however, Q_{rad}/Q_{chem} decreases to values that are typically about 0.1 or less. This decrease occurs at about the time when visible soot radiation and fiber glowing cease to be evident in the video records.

Note that burning rates were observed to decrease in the FSDC-1 and FSDC-2 experiments as droplets became larger, with the largest droplet exhibiting burning-rate constants roughly 50% lower than the smaller droplets (before flame contraction). This trend may be a result of radiant heat loss effects,[13,15,16,20–23] and the present results suggest that nonluminous radiant losses may be more important than luminous radiant heat losses in determining burning rates. For example, the data presented here show that smaller droplets had higher burning rates even though these droplets had higher fractional radiant heat loss rates. The smaller droplets displayed more soot, and it is likely that the enhanced radiant emissions were from soot particles located between droplets and flames. From thermophoresis, soot particles are driven from the primary reaction zone to cooler regions near the droplet surface such that significant radiant losses from soot may occur far from the primary reaction zone. In contrast, molecular band emissions will arise from species that exist on both sides of the flame zone as well as in the flame zone itself, leading to cooling of the flame, and so it is reasonable to expect that nonluminous radiation will play a stronger role in determining chemical heat release rates and burning rates, at least when soot does not penetrate the reaction zone in significant amounts.

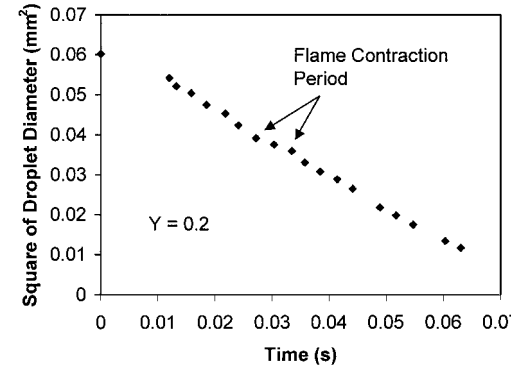

Fig. 8 Droplet diameter data for heptane/hexadecane droplets burned in simulated reduced gravity ($Y = 0.2$ and $d_0 = 0.25$ mm).

Recall that the rad 2 measurements detected radiant heat losses in an H_2O radiant emission wavelength band (5.1–7.2 μm). If there were no other contributors to the radiant power detected by rad 2 in this band, then it would be reasonable to expect that Q_{rad}/Q_{chem} would be larger for larger initial droplet diameters if Q_{rad} were determined using the data from rad 2. Analysis of the data shows that this is not the case, however. In the experiments with smaller droplets described here, radiant heat losses from soot were present. Because soot emissions are continuous, that is, not concentrated in bands, a portion of the radiant emissions from soot will be in the rad 2 wavelength range. In the present case, it is estimated using known spectral behaviors of soot that about 10% of the total soot radiant emissions were in the rad 2 wavelength range. Because energy loss rates via soot radiant emissions should be large relative to molecular band radiation energy losses (for smaller droplets), this can easily produce significant increases in the rad 2 measurements for smaller droplets that produce soot, leading to values of Q_{rad}/Q_{chem} that are larger for smaller droplets as observed in the present experiments (where Q_{rad} is based on the rad 2 data).

Finally, droplet diameter data from the present contoured-tube experiments are shown in Fig. 8. These data show a decrease in burning rates at the time of the flame contraction, which was readily apparent (via visual observations of the flames) in the experiments. The initial droplet diameter, that is, the data at the time of 0 s, was measured under cold flow conditions before injection of the droplet stream into the contoured-tube hot gas environment. Droplet diameter data are not shown between 0 and 0.01 s because equipment limitations did not allow droplets to be imaged in this initial portion of the flow tube.

Estimates of Liquid Species Diffusion Coefficients

Flame contraction occurs as a result of sudden droplet heating (and, thus, decreased vaporization) at a time when the mass fraction of the low-volatility component in the liquid at the surface rapidly approaches unity. Theory[9,10] neglecting liquid-phase convection

predicts that the ratio of d_0 to d_c is a function of the initial low-volatility mass fraction Y in the droplet and the parameter $\varepsilon = 8D/K_1$, where D is the liquid species diffusivity and K_1 the burning-rate constant (i.e., the negative of the slope of the d^2–t plot) before flame contraction. Under typical conditions, $\varepsilon \ll 1$. Note that in some cases the d^2–t plots showed curvature before flame contraction. In these cases, the K_1 values were taken to be the slope of the d^2–t plot before the flame contraction. When extinction occurred, it was assumed to be caused by flame contraction, and the slope of the d^2–t plot before extinction was used to estimate K_1. This assumption is based on the observation that extinction occurred at times where flame contractions were expected.

Theory[10] predicts that a flame contraction will occur when Eq. (5) is satisfied:

$$1 + h_0 + \varepsilon h_1 + H_0/\varepsilon + H_1 + \varepsilon H_2 - h_{\text{match}} = 1/Y \qquad (5)$$

The following variables are used in Eq. (5):

$$h_0 = \phi\left[1 + \text{erf}\left(\phi^{\frac{1}{2}}/2\right)\right]/2 + \text{erf}\left(\phi^{\frac{1}{2}}/2\right) + (\phi/\pi)^{\frac{1}{2}} e^{-\phi/4}$$

$$h_1 = 4 + \phi + 3\phi^2/2 - 2e^{-\phi/4} + (2 + \phi/2 + 3\phi^2/4)\left[\text{erf}\left(\phi^{\frac{1}{2}}/2\right) - 1\right] + e^{-\phi/4}(\phi/\pi)^{\frac{1}{2}}(3\phi/2 - 2)$$

$$H_0 = (e^{3\tau} - 1)/3, \qquad H_1 = (e^{3\tau} + 2)/3$$

$$H_2 = \tfrac{22}{9} + \left(\tfrac{14}{9} - 24\tau/9\right)e^{3\tau}$$

$$h_{\text{match}} = 1 + \tau/\varepsilon + \varepsilon[4 + \tau/\varepsilon + 3\tau^2/(2\varepsilon^2)]$$

In addition, $\tau = \ell n(d_0/d)$ is a dimensionless time and $\phi = \tau/\varepsilon$ a rescaled time. Equation (5), when combined with experimental data on flame contractions, provides estimates of effective liquid species diffusivities in the droplets. Specifically, experimental data yield the ratio d_0/d_c, which defines $\tau = \tau_c$ at the onset of the flame contraction so that the value of ε and, hence, D can be obtained from the equations.

In applying this method, the initial droplet volumes (from the experiments) are increased by about 10% to account approximately for the droplet swelling that occurs after ignition. The assignment of a 10% increase in the droplet volume is motivated by the fact that droplets heat up to temperatures close to their boiling points after ignition (and typically before significant droplet surface regression occurs). Because these droplets were initially mostly heptane, volume changes from droplet heatup were assumed to be caused by heatup of droplets from the ambient temperature to temperatures close to the boiling point of heptane. The density of heptane decreases by about 10% over these limits, which leads to an increase in droplet volume of about 10%. Inserting this modified value of τ_c into Eq. (5) yields (after iteration) a unique value for ε. The results for ε were not strongly sensitive to the value used for the percentage decrease in the liquid density; typically, ε would vary by up to 20% as the droplet density was varied by values up to 10%. This ε, together with the K_1 obtained from the experimental data, produces a value of the liquid-species diffusivity D that is appropriate for each experiment. Table 1 lists the values of ε and D estimated in this way to apply to these experiments. Figure 9 (Ref. 24) shows the resulting deductions of D as a function of the initial hexadecane mass fraction Y. For comparison, results from previous drop tower experiments[10] and normal-gravity experiments[8] on combustion of heptane/hexadecane droplets at 1 atm are also shown in Fig. 9. The normal-gravity experiments[8] involved injecting heptane/hexadecane droplets into the postcombustion gases of a flat-flame burner, whereas the drop-tower experiments[10] involved combustion of heptane/hexadecane droplets in air or other ambients. The D values for these experiments were inferred using flame contraction data and the methodology described earlier.

Note that the identification of τ_c from experimental data involves some uncertainty because of factors such as fuel vapor accumulation, gas-phase transient diffusion, droplet heatup, and that flame contraction, while usually an abrupt event, does take a finite time to occur, which leads to some uncertainty about the onset time for

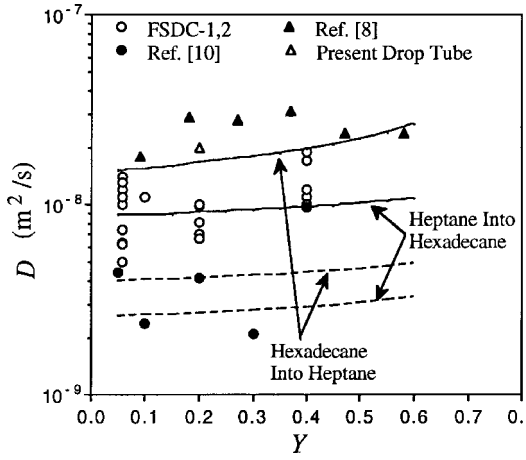

Fig. 9 Estimated species diffusion coefficients D [estimated using Eq. (1)] vs initial hexadecane mass fraction Y; solid lines are D values obtained from correlations,[24] where droplet temperatures were estimated using Eq. (6); dashed lines are D values obtained from correlations,[24] where droplet temperatures were assumed to be at the boiling point T_b of the initial heptane/hexadecane mixture.

flame contraction. However, the time difference between the onset of a plateau and the onset of the gas-phase flame contraction is generally not large. In the data reduction, the τ_c values are defined as the dimensionless times when a plateau begins. When a flame was visible, the flame data were used in conjunction with d^2–t data to determine the onset of a plateau. The radiometer data were also sometimes useful in this regard. There is clearly some uncertainty, however, in making these determinations (for the reasons stated). The uncertainty in the experimental definition of τ_c contributes to the overall uncertainty in the estimates of D, which is estimated to be as large as about a factor of two when uncertainties in the various experimental variables are taken into account.

Note that the test 18 data ($Y = 0.40$) in Table 1 correspond to the one instance where a droplet was placed in a convective flow. As would be expected, this droplet exhibited the largest K_1 value. The D value estimated for this droplet is similar to liquid species diffusivity values calculated for the other $Y = 0.40$ data. This suggests that the external convective flow did not play a significant role in determining the onset time for flame contraction.

Even though the uncertainties in the liquid diffusivities values may be as large as about a factor of two, it is evident in Fig. 9 that there are significant variations between the D values estimated to apply to the different experiments. The largest D values are calculated to apply to the 1-g experiments, with the FSDC-1 and FSDC-2 D values lying below those calculated to apply to the 1-g experiments and the drop tower experiments. These differences may be from variations in droplet internal convective flows as well as differences in droplet temperatures.

The 1-g experiments[8] were performed by injecting droplets into convective environments. The droplet formation and injection processes would have caused shear stresses to exist in the liquid, which would lead to droplet internal flows. As shown elsewhere,[25] characteristic times for viscous decay of internal flows inside of a droplet are quite long (of the order of the lifetime of a burning droplet), and as a result the droplets studied in 1-g may not have had time to approach an internally quiescent state before ignition or during the droplet lifetime. Also note that gas-phase convective flows were present in the 1-g experiments[8] such that spherical symmetry in the gas phase was likely not approached as well. Contoured flow tubes are required to reduce buoyant and forced convective flows to negligible levels using the injected droplet technique such that spherical symmetry is approached in the gas phase.[18] However, even when contoured tubes are used, the internal droplet flows associated with the droplet formation processes can still remain, as indicated by the results from the present contoured-tube experiments. Specifically, the contoured-tube data in Fig. 8 yield $D = 1.95 \times 10^{-9}$ m^2/s, which lies close to (and slightly below) the D values deduced from the injected droplet results from the 1-g experiments.[8]

Other normal-gravity experiments to measure liquid species diffusion rates in droplets have been performed in convective environments.[3] These experiments were also performed by injecting droplets into a hot zone where they burned. The theory that was applied to calculate D values assumed that spherical symmetry existed in the gas and liquid phases. A conclusion of this study was that liquid-phase species diffusion in droplets may be more rapid than predicted by theory.[3] However, these experiments likely did not approach spherical symmetry in the gas phase, and they may not have had a spherically symmetrical liquid phase. (A piezoelectric droplet generator was used.) Thus, the liquid diffusion coefficients that were estimated to be applicable to these experiments would have been influenced by convective transport. It is probable that droplet internal flows are more intense for the case where droplets are injected piezoelectrically relative to the microgravity experiments described here, which employed an opposed-needle deployment method.

It is not clear why the drop tower data show smaller D values than the FSDC-1 and FSDC-2 data. One possible reason is that the drop tower experiments utilized 12-μm SiC support fibers, whereas the FSDC-1 and FSDC-2 experiments employed SiC support fibers that were about an order-of-magnitude thicker. The thicker fibers would have promoted greater heat transfer rates along the fiber, which would lead to more intense thermocapillary flows and, hence, larger effective D values. Another possible reason is that the conditions before ignition of the droplets were different. As has been shown elsewhere,[25] decay of internal flows within droplets can take substantial amounts of time. Variations in initial droplet internal flowfields could easily lead to significant differences in mixing rates inside droplets and, hence, differences in effective liquid species diffusivities. The ignition methods were also different in that the FSDC-1 and FSDC-2 experiments utilized hot wires, whereas spark ignition, which is much more rapid, was employed in the drop-tower experiments.[10] Differences in ignition methods could potentially lead to variations in internal flows, for example, from capillary flows associated with generation of droplet surface temperature gradients during the ignition transients. Different ignition methods could also lead to variations in gas-phase temperature fields, which could play a role in determining combustion behaviors.

Droplet temperatures can also affect liquid species diffusivities. Following droplet ignition, the droplet surface temperature will closely approach the saturation temperature of the liquid mixture at the surface before appreciable liquid vaporization commences. Following this, droplet temperatures will increase as the mass fraction of hexadecane at the liquid surface builds. Estimates[9,10] indicate that after this initial droplet heat up period and before flame contraction, the dimensionless droplet interior temperature T_c at the onset of flame contraction may be estimated using

$$T_c = T_0 + \left(RT_0^2/L\right)\ln[1 + \omega(1 - \beta')/\beta'] \qquad (6)$$

In Eq. (6), ω is the ratio of the molecular weights of the high-volatility and low-volatility components, L is the enthalpy of vaporization of the high-volatility component, R is the gas constant of the high-volatility component, T_0 is the initial droplet interior temperature assuming that droplet heatup is complete, and β' is a small parameter representing the ratio of a characteristic time for droplet temperature changes to a characteristic time for droplet size changes (before flame contraction). Typical values of ω and β' are such that $\ln[1 + \omega(1 - \beta')/\beta']$ is in the range 3–4. (We used a value of 3.6.)

It is appropriate to compare the diffusion coefficients in Table 1 with data on diffusivities from the literature evaluated at the temperature T_c. Such results are shown as the solid lines in Fig. 9, where, in using Eq. (6), T_0 has been approximated as the boiling temperature T_b of the initial heptane/hexadecane mixture. Variations in T_b are not large over the range of Y considered, and, as a result, the calculated liquid-species diffusivities do not vary appreciably. The dashed lines in Fig. 9 are for the case where diffusion coefficients were calculated at T_b, which provides a reasonable lower bound on droplet temperatures. For all of the lines in Fig. 9, diffusion coefficients were calculated using correlations from the literature.[24] The diffusion coefficients in Fig. 9 correspond to the limiting cases of infinite dilution of heptane in hexadecane, or hexadecane in heptane. As is typical in liquid diffusion, species diffusivities depend on the mole fraction of each component, and species diffusivities for finite dilutions are expected to lie between these infinite-dilution limits for the present alkane mixtures. (Note that, in highly nonideal mixtures, species diffusivities for finite dilutions may lie outside the infinite-dilution limits.) For the present calculations, differences between the two limiting cases are not large and are of the order of the estimated uncertainty for the present experiments.

Except for the $Y = 0.4$ data point, the drop-tower data in Fig. 9 compare reasonably well with the D values calculated assuming that droplets are at T_b. The drop-tower experiment at $Y = 0.4$ exhibited significant bubble beneration in the liquid, which can explain the higher D value, that is, the bubbling would have enhanced liquid mixing rates. In contrast, the data for FSDC-1, FSDC-2, and the 1-g injected droplet experiments[8] compare better with the D values calculated assuming that droplet temperatures are described by Eq. (6). If Eq. (6) provides a good description of droplet temperatures at the onset of flame contraction, then it is not clear why the drop-tower D values and a significant number of the FSDC-1 and FSDC-2 D values fall below the diffusivity values calculated using Eq. (6). A likely explanation is that Eq. (6) overpredicts droplet temperatures somewhat and that differences in droplet internal circulation rates are responsible for the variations in D values both within and between the data sets. To verify this hypothesis, however, data are needed on droplet temperatures and droplet interior flowfields. Unfortunately, sufficient data are not presently available. Obtaining such data, however, would provide important information on how droplet interior flows affect droplet behaviors.

Conclusions

This research has shown that effective liquid species diffusivities inferred from experimental data on flame contraction can vary significantly between experiment sets. The variations are likely a result of differences in internal circulation patterns and possibly droplet temperature variations. Such variations are relevant to large droplets such as those investigated here, as well as to spray-size droplets (which can also exhibit variations in internal flow patterns) used in combustion devices. For example, calculations relevant to spray conditions have shown that the state of the liquid-phase convective flowfield (and the resulting effective liquid species diffusivity) can significantly affect behaviors of individual bicomponent droplets[6] as well as bicomponent sprays.[7]

Although the present experiments focused primarily on large droplets, note that liquid phase behaviors, for example, effective liquid diffusivities, should scale from large droplets to small droplets, provided the internal flowfields are similar. For example, theory to predict the onset of flame contraction[9,10] predicts that d_c scales linearly with d_0 for ε and Y held constant, implying that effective diffusivities should be the same for large droplets (such as those studied here) and small droplets of practical concern, provided the internal flowfields are similar. Droplet internal flows could not be quantitatively evaluated in the present experiments. However, it would be beneficial to obtain data on droplet internal flowfields using flow visualization techniques so that effective liquid diffusivities could be related to the actual conditions within droplets. This would allow the effects of liquid circulation patterns on effective species diffusivities to be quantitatively evaluated.

The data presented also show that sooting and radiant heat losses varied strongly with the initial droplet size. Initially larger droplets exhibited higher radiant heat losses at early times than initially smaller droplets. At later times, however, radiant heat losses from larger droplets decreased to low values when droplet flame sizes became larger (and cooler) and soot radiation was no longer evident in the video records. The radiometer data also indicate that for the droplets studied here, molecular band radiation may be more important in determining burning-rate and extinction behaviors than radiant heat losses from soot particles. Although of fundamental interest, these observations are also useful for validating models to predict phenomena such as extinction, radiant heat losses, and burning rates. The practical usefulness of this rests on the idea that when theory agrees with fundamental experiments such as those considered here, then predictions can be made with greater confidence

for situations where accurate experimental data are not available, for example, practical combustion systems. Also note that the results described here are potentially relevant to spacecraft fire safety in that sooting decreased as droplet flames became larger, which is contrary to many normal gravity results. In addition, the spectral (radiant emission) characteristics of the flames changed as their sizes increased. These characteristics may be present in other microgravity flames, and as such space-based fire detection techniques may need to take these behaviors into account.

In addition to the liquid-phase flow visualization experiments just mentioned, future experiments should also provide spectrally resolved radiometer data. Ideally, these data should be spatially and temporally resolved. Such measurements would allow radiating species to be identified, and soot temperatures and gas phase temperatures could be inferred using optical pyrometry techniques. These measurements would increase understanding of the relative roles of luminous and nonluminous radiant losses on combustion phenomena. It is also important to perform experiments with equipment that allows for imaging of weak flames, for example, imaging of emissions from OH radicals via intensified charge-coupled device cameras. This would provide unambiguous indications of the occurrence of flame contraction, which was difficult to detect with the larger droplets studied in the present Spacelab experiments. Finally, the theory to predict flame contraction can be improved, for example, by incorporating radiant heat losses into the model.

Acknowledgments

This research was supported by the NASA Microgravity Combustion Science program. Thanks are extended to the USML-2 and MSL-1 crewmembers, in particular R. Crouch, F. Leslie, D. Thomas, and K. Thornton, who performed the flight experiments, and M. Lopez-Alegria for repair of the FSDC-1 apparatus. Thanks are also extended to personnel at the Payload Operation Control Center at NASA Marshall Spaceflight Center in Huntsille, Alabama, for support and suggestions. Glovebox facility personnel and the participation of M. King, B. Quigley, and H. Ross were indispensable. NASA John H. Glenn Research Center at Lewis Field personnel, particularly C. Fritz, S. Motil, and J. Parina, are acknowledged for their efforts with flight hardware. Fellow FSDC-1 and FSDC-2 investigators R. Colantonio; D. Dietrich; F. Dryer; J. Haggard Jr.; V. Nayagam; and F. Williams are acknowledged for their support. Appreciation is expressed to D. Dietrich and J. Rankin for efforts related to data analysis.

References

[1]Dwyer, H. A., "Calculations of Droplet Dynamics in High Temperature Environments," *Progress in Energy and Combustion Science*, Vol. 15, No. 2, 1989, pp. 131–158.

[2]Hanson, S. P., Beer, J. M., and Sarofim, A. F., "Non-Equilibrium Effects in the Vaporization of Multicomponent Fuel Droplets," *Nineteenth Symposium (International) on Combustion*, Combustion Inst., Pittsburgh, PA, 1982, pp. 1029–1036.

[3]Randolph, A. L., Makino, A., and Law, C. K., "Liquid-Phase Diffusional Resistance in Multicomponent Droplet Combustion," *Twenty-First Symposium (International) on Combustion*, Combustion Inst., Pittsburgh, PA, 1986, pp. 601–608.

[4]Megaridis, C. M., "Liquid-Phase Variable Property Effects in Multicomponent Droplet Evaporation," *Combustion Science and Technology*, Vol. 92, Nos. 4–6, 1993, pp. 291–311.

[5]Talley, D. G., and Yao, S. C., "A Semi-Empirical Approach to Thermal and Composition Transients Inside Vaporizing Fuel Droplets," *Twenty-First Symposium (International) on Combustion*, Combustion Inst., Pittsburgh, PA, 1986, pp. 609–616.

[6]Sirignano, W. A., "Fluid Dynamics and Transport of Droplets and Sprays," Cambridge Univ. Press, Cambridge, England, U.K., 1999, Chap. 3.

[7]Aggarwal, S. K., "Further Results on Evaporating Bicomponent Fuel Sprays," *International Journal of Heat and Mass Transfer*, Vol. 31, No. 12, 1988, pp. 2593–2597.

[8]Wang, C. H., Liu, X. Q., and Law, C. K., "Combustion and Microexplosion of Freely-Falling Multicomponent Droplets," *Combustion and Flame*, Vol. 56, No. 2, 1984, pp. 175–197.

[9]Shaw, B. D., and Williams, F. A., "Theory of Influence of a Low-Volatility, Soluble Impurity on Spherically Symmetric Combustion of Fuel Droplets," *International Journal of Heat and Mass Transfer*, Vol. 33, No. 2, 1990, pp. 301–317.

[10]Aharon, I., and Shaw, B. D., "Estimates of Liquid Species Diffusivities from Experiments on Reduced-Gravity Combustion of Heptane–Hexadecane Droplets," *Combustion and Flame*, Vol. 113, No. 4, 1998, pp. 507–518.

[11]Yang, J. C., and Avedisian, C. T., "The Combustion of Unsupported Heptane–Hexadecane Mixture Droplets at Low Gravity," *Twenty-Second Symposium (International) on Combustion,* Combustion Inst., Pittsburgh, PA, 1988, pp. 2037–2044.

[12]Mikami, M., Kono, M., Sato, J., Dietrich, D. L., and Williams, F. A., "Combustion of Miscible Binary-Fuel Droplets at High Pressure Under Microgravity," *Combustion Science and Technology*, Vol. 90, Nos. 1–4, 1993, pp. 111–123.

[13]Dietrich, D. L., Haggard, J. B., Jr., Dryer, F. L., Nayagam, V., Shaw, B. D., and Williams, F. A., "Droplet Combustion Experiments In Spacelab," *Twenty-Sixth International Symposium on Combustion*, Combustion Inst., Pittsburgh, PA, 1996, pp. 1201–1207.

[14]Dietrich, D. L., Haggard, J. B., Jr., Nayagam, V., Dryer, F. L., Shaw, B. D., and Williams, F. A., "Fiber-Supported Droplet Combustion," *Second United States Microgravity Laboratory: One Year Report, Volume 2*, NASA/TM -1998-208697/VOL2, 1998, pp. 32-523–32-536.

[15]Colantonio, R., and Nayagam, V., "Radiative Heat Loss Measurements During Microgravity Droplet Combustion," *Proceedings of the 1997 Technical Meeting of the Central States Section of the Combustion Institute*, Combustion Inst., Pittsburgh, PA, 1997, pp. 125–129.

[16]Marchese, A. J., Dryer, F. L., and Nayagam, V., "Numerical Modeling of Isolated *n*-Alkane Droplet Flames: Initial Comparisons with Ground and Space-Based Microgravity Experiments," *Combustion and Flame*, Vol. 116, No. 3, 1999, pp. 432–459.

[17]Colantonio, R., Dietrich, D. L., Haggard, J. B., Jr., Nayagam, V., Dryer, F. L., Shaw, B. D., and Williams, F. A., "Fiber-Supported Droplet Combustion-2 (FSDC-2)," *Microgravity Science Laboratory (MSL-1) Final Report*, NASA CP -1998-208868, 1998, pp. 141–155.

[18]Wang, D. F., and Shaw, B. D., "Droplet Combustion in a Simulated Reduced-Gravity Environment," *Combustion Science and Technology*, Vol. 113–114, 1996, pp. 451–470.

[19]Chen, A. G., and Shaw, B. D., "Laser Attenuation Measurements of Soot Volume Fractions During Reduced-Gravity Combustion of Heptane and Heptane/Hexadecane Droplets," *Combustion Science and Technology*, Vol. 150, Nos. 1–6, 2000, pp. 59–76.

[20]Marchese, A. J., and Dryer, F. L., "The Effect of Non-Luminous Thermal Radiation in Microgravity Droplet Combustion," *Combustion Science and Technology*, Vol. 124, Nos. 1–6, 1997, pp. 371–402.

[21]Nayagam, V., Haggard, J. B., Jr., Colantonio, R. O., Marchese, A. J., Dryer, F. L., Zhang, B. L., and Williams, F. A., "Microgravity *n*-Heptane Droplet Combustion in Oxygen–Helium Mixtures at Atmospheric Pressure," *AIAA Journal*, Vol. 36, No. 8, 1998, pp. 1369–1378.

[22]Chao, B. H., Law, C. K., and T'ien, J. S., "Structure and Extinction of Diffusion Flames with Flame Radiation," *Twenty-Third Symposium (International) on Combustion*, Combustion Inst., Pittsburgh, PA, 1990, pp. 523–531.

[23]Saitoh, T., Yamazaki, K., and Viskanta, R., "Effect of Thermal Radiation on Transient Combustion of a Fuel Droplet," *Journal of Thermophysics and Heat Transfer*, Vol. 7, No. 1, 1993, pp. 94–100.

[24]Erkey, C., Rodden, B., and Akgerman, A., "A Correlation for Predicting Diffusion Coefficients in Alkanes," *Canadian Journal of Chemical Engineering*, Vol. 68, No. 4, 1990, pp. 661–665.

[25]Shaw, B. D., and Chen, A. G., "Observation of Flows Inside Droplets Undergoing Combustion in Reduced Gravity," *Microgravity Science and Technology*, Vol. 10, No. 3, 1997, pp. 136–143.

J. R. Bellan
Associate Editor